Analysis of the overlap section in a high-speed railway catenary by means of numerical simulations

S. Gregori*, J. Gil, M. Tur, J.E. Tarancón, F.J. Fuenmayor

Instituto Universitario de Ingeniería Mecánica y Biomecánica (I2MB)
Universitat Politècnica de València
Camino de Vera s/n, 46022 Valencia, Spain

Abstract

The transition between catenary tensioning sections is accomplished smoothly by overlapping a number of spans in each catenary section. This work presents an analysis of the overlap section in a high-speed railway catenary based on numerical simulations. The paper studies the influence on the system's dynamic behaviour of features such as double cantilevers and tensioning devices efficiency. Four and five-span overlaps are compared and the effect of train speed and overlap contact wire geometry are also analysed. Finally, an entire catenary section is optimised by Bayesian Optimisation techniques, leading to a catenary configuration with an interaction force with a standard deviation notably lower than that provided by the nominal catenary design.

Keywords: Railway catenary, Overlap section, Multiple pantograph operation, Tensioning device, Bayesian Optimisation

1. Introduction

High-speed railway vehicles are powered by electric energy transmitted through the interaction of the overhead contact line or catenary and pantograph. The

*Corresponding author
Email addresses: sangreve@upv.es (S. Gregori), jaigiro@etsid.upv.es (J. Gil), manuel.tur@mcm.upv.es (M. Tur), jetaranc@mcm.upv.es (J.E. Tarancón), ffuenmay@mcm.upv.es (F.J. Fuenmayor)

quality of the power supply is extremely sensitive to this interaction, which is responsible for contact loss and wear on the sliding components.

Catenaries are installed as a sequence of sections about [1-1.5] km long with tensioning devices at each end composed of weights and pulleys whose purpose is to guarantee constant mechanical tension on the wires. The transition from one section to another is made progressively with the overlapping of certain spans in which the contact wire of one section is raised while that of the upcoming section is lowered to the nominal height. These overlap sections, in which the pantograph interacts with two wires simultaneously, are thus critical to the quality of the power supply [1], measured in terms of statistical parameters of the interaction force such as its standard deviation (SD), its maximum and its statistical minimum.

Simulations of the pantograph-catenary dynamic interaction are now widely used and well established, as can be seen in the state-of-the-art literature [2, 3, 4]. Most studies which have been performed to analyse the dynamic behaviour of the system focus on the central part of the catenary section. Although some of the analyses deal with curved paths [5], very few consider transitions between catenary sections. Among these, Shimizu et al. [6], provide some experimental measures of contact wire height and wear on overlapping sections of the Japanese high-speed Shinkansen lines in a study that evaluated different simulated scenarios for contact wire height variations in overlaps. Harèll et al. [7, 8] proposed a finite element model of a catenary with a five-span overlap section and suggested that the dynamic behaviour at the transition can be even better than in the central spans. These results show that the dynamic performance of the overlap sections is improved by lowering the lift at the supports. Massat et al. [9] proposed a finite element-based tool able to deal with pantograph-catenary interaction in overlap sections and evaluate its elasticity. Mei et al. [10] also used finite element simulations considering five-span overlap sections. Benet et al. proposed an academic 2D model [11] composed of a single transition span with droppers only in the first half, and used this to provide the results of a dynamic simulation. More recently, Antunes et al. [12] analysed the dynamic behaviour

of the overlap sections and concluded that the impact of different overlapping arrangements is still a challenge to be considered.

The main objective of this work is to address this challenge by proposing a method of analysing different overlap arrangements and optimising the geometry of the overlap section of high-speed catenaries by numerical simulations of the pantograph-catenary interaction. A model based on the EAC-350 catenary was chosen as an example, although the proposed methods could also be applied to other catenary types. The methods proposed in previous work [13, 14, 15] are used as the basis for constructing a numerical model of the catenary. In the present work the model is extended to incorporate transition spans and the fast simulation solver [14] is modified to consider interaction of the pantograph with two contact wires. The paper analyses the effect of other features, such as double cantilevers and tensioning device efficiency, which are usually neglected in numerical models.

The paper is organised as follows. After this Introduction, the extension of the numerical model presented in [15] to consider overlap sections is described in Section 2. The effect of double cantilevers and changes in tensioning device efficiency is dealt with in Section 3. In Section 4 current collection quality in the overlap sections is analysed at different train speeds and compared with that obtained in the central spans. A parametric analysis of the contact wire height profile in transition spans is performed in Section 5, while Section 6 contains a comparison between three, four and five-span overlaps. In Section 7, a Bayesian Optimisation (BO) algorithm is used to efficiently obtain the optimum contact wire height and dropper spacing of an entire catenary section, including the overlap, in terms of the interaction force SD. Some concluding remarks are given in Section 8.

2. Numerical models

The catenary model was based on the EAC-350 overhead contact line, a high-speed railway catenary whose material properties and geometric parameters can

be found in the Appendix of [15]. The finite element (FE) model used in this work is developed from the previous works [13], which presents how the static configuration is obtained, and [14] in which an efficient dynamic simulation procedure is proposed.

In this FE catenary model, posts and cantilevers were replaced by appropriate boundary conditions. The steady arms, messenger and contact wire ends are pinned, whilst the vertical coordinate of the messenger wire connections to the supports are fixed. There are two different posts in a catenary section that need additional boundary conditions. The central mast is anchored and has restricted longitudinal movement (circle in Figure 1), while the first and last cantilevers prevent the vertical displacement of the contact wire (fixed brackets marked with a cross in Figure 1).

This section highlights the particular features and new input parameters needed to include transition spans at the beginning and end of a catenary section, as shown in Figure 1. The non-linear shape-finding problem is solved to obtain the initial catenary configuration while fulfilling the equilibrium equations and constraints defined by the design, as described in [13] and similarly presented in [16].

The reader is referred to [13] for details of the implementation. Here, we only define the new constraints used to incorporate overlap spans into the catenary model (see Figure 2). The new input parameters are defined in Table 1.

Static equilibrium is established by equating internal elastic $\mathbf{F_{int}}$, and gravity $\mathbf{F_g}$ forces:

$$\mathbf{F_{int}}(\mathbf{q}, \mathbf{l}) - \mathbf{F_g}(\mathbf{l}) = \mathbf{0} \tag{1}$$

which depends on the nodal coordinates $\mathbf{q}$ and the undeformed lengths of the elements $\mathbf{l}$.

The geometric parameters h_1, h_{sup}, h_{cw}^{td} and h_{mw}^{td} (see Figure 2) are defined as boundary conditions, including the fixed bracket, which is modelled by restricting the vertical movement of the contact wire support at height h_1. Other parameters of the overlap section are imposed as constraints of the shape-finding

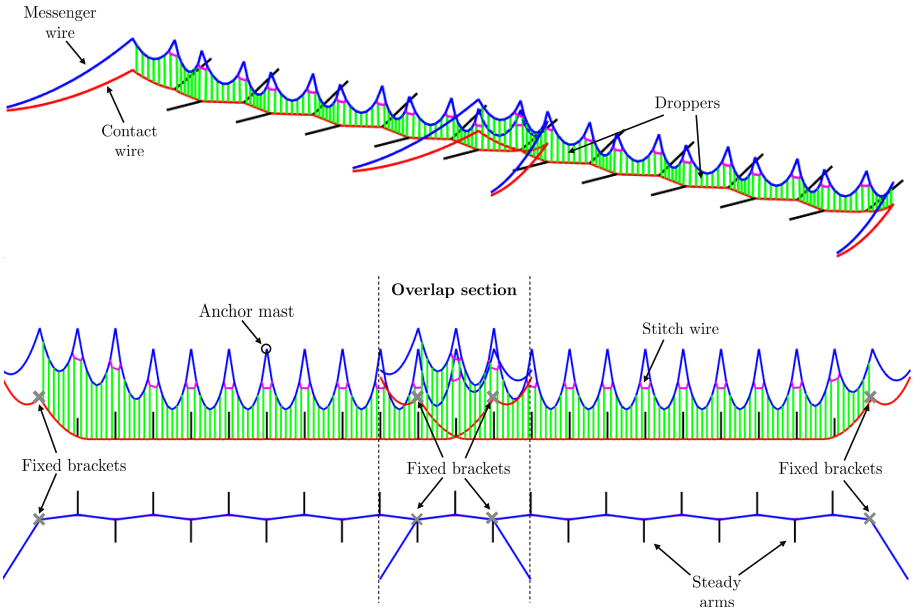

Figure 1: *Catenary model with a four-span overlap and its principal elements viewed from different perspectives.*

problem:

- The vertical coordinate h_2 of the node that connects the steady arm with the contact wire. This is accomplished by including the steady arm support height $\mathbf{h_{sa}}$ as a new unknown in the initial configuration problem. Although not visible in Figure 2, the lateral coordinate of this point is also considered to obtain the desired stagger in the contact wire. The result of these constraints determines the inclination of the steady arm.

- The vertical coordinate h_d of the nodes that connect the dropper d with the contact wire. Each undeformed dropper length $\mathbf{l_d}$ is set as the unknown by which it can be achieved.

  Different profiles of this span can be defined by imposing the height of each yellow circle in Figure 2. The parabola used passes through the support heights h_1 and h_2 and is tangent to the nominal height h_0.

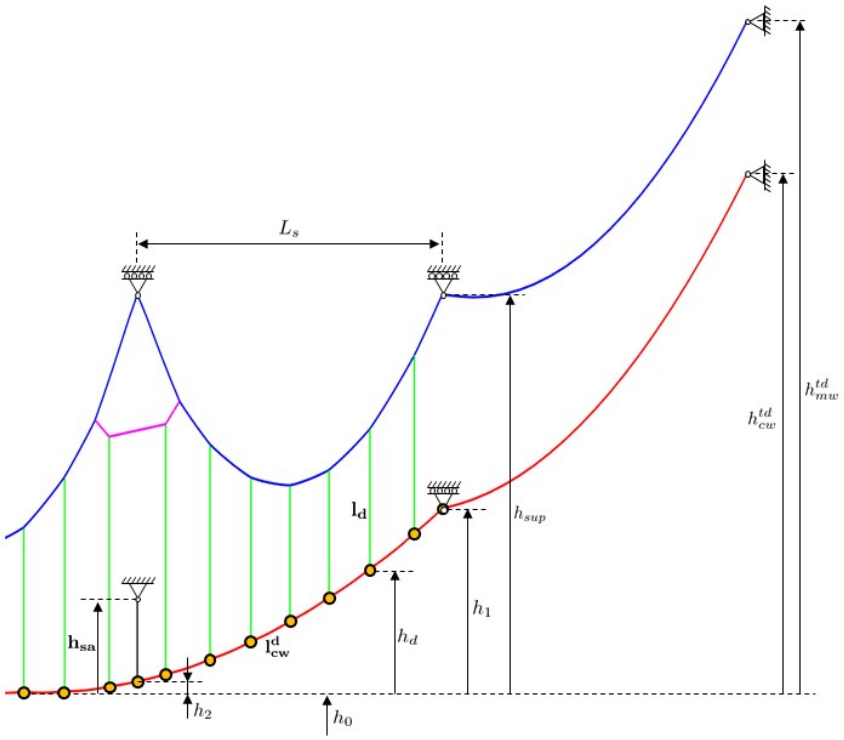

Figure 2: *Front view of the overlap spans. Parameters (plain symbols) and variables (bold symbols) that define the initial configuration.*

As an example of the results that can be obtained from the initial configuration problem, Figure 3 shows the tension forces of each of the seven droppers f_d of the last four spans of a catenary section. The input parameters to define the initial configuration of the overlap section are given in Table 1. Droppers in the first two spans hold a tensile force around 110 N and the pattern observed is repeated in all central spans. However, in the overlap spans (the two last spans considered in Figure 3) in which the contact wire is raised, droppers are notably less tensioned.

Once the initial configuration is available a linearised dynamic equation is obtained since displacements $\mathbf{u}$ can be considered small in the dynamic problem. This leads to:

$$\mathbf{M\ddot{u} + C\dot{u} + Ku = F} \tag{2}$$

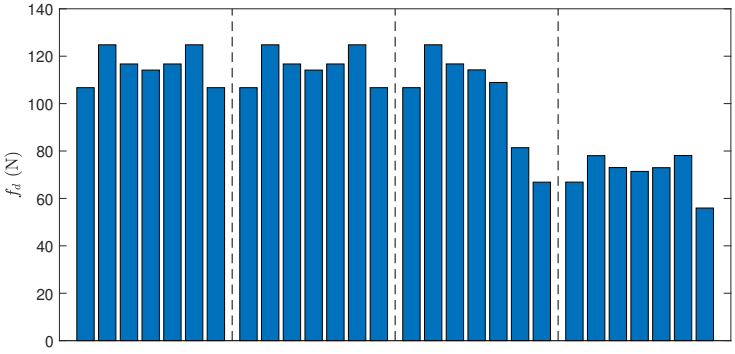

Figure 3: *Tension force of droppers on the last four spans with droppers in a catenary section.*

Table 1: *Input parameters to define the initial configuration of the overlap section.*

Parameter	Symbol	Value
Distance between poles	L_s	65 m
Nominal height	h_0	5.3 m
Contact wire tensioning device height	h_{cw}^{td}	7.3 m
Messenger wire tensioning device height	h_{mw}^{td}	8.2 m
Messenger wire support height	h_{sup}	6.6 m
Contact wire support 1 height	h_1	0.6 m
Contact wire support 2 height	h_2	0.035 m

in which $\mathbf{M}$ and $\mathbf{K}$ are the mass and the stiffness matrices, respectively, matrix $\mathbf{C}$ is built by a Rayleigh damping model whose damping coefficients are taken from the benchmark exercise [2], $\mathbf{F}$ denotes the vector of external applied forces and $\ddot{\mathbf{u}}$ and $\dot{\mathbf{u}}$ are the nodal accelerations and velocities, respectively. Despite this standard appearance, the problem entails two non-linearities related to dropper slackening (droppers only transmit traction forces) and pantograph contact sliding and potential contact loss, which have to be considered to obtain realistic results.

The pantograph is modelled by a lumped mass model, as seen in Figure 4a.

This model only introduces vertical displacements and the movement of the three masses is linearised with respect to the coordinate z_{ref}. The external force f_{ext}, applied to the bottom mass of the model, simulates the action of the up-lift mechanism. All the values which define the pantograph model can be found in [15].

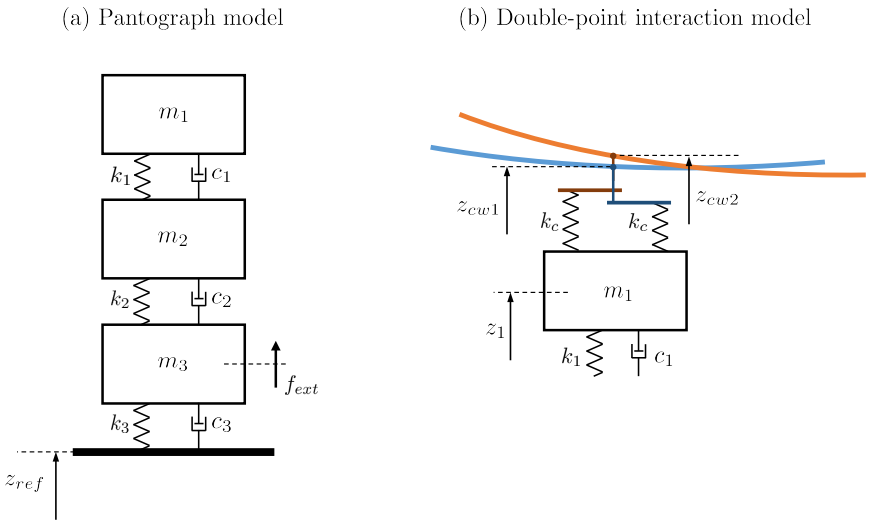

Figure 4: *(a) Lumped mass pantograph model. (b) Double-point interaction penalty model.*

To model the pantograph-contact wire interaction a penalty stiffness is introduced at the interaction point to couple both models, which, according to [17] is set to $k_c = 50$ kN. As schematically depicted in Figure 4b, when the pantograph passes through the overlap section, there will be two interaction points, one for each contact wire, which are on the same coordinate, so that in the case of double contact the original formulation from [14] must be modified. In this case, the total interaction force of the j-th pantograph f_{int}^{j} is found by totalling the interaction forces of the two contact wires f_{int}^{j1} and f_{int}^{j2} so that:

$$f_{int}^{j} = f_{int}^{j1} + f_{int}^{j2} = k_c \left(z_1 - z_{cw1} + z_1 - z_{cw2} \right) \tag{3}$$

where z_1 is the absolute height of the upper mass of the pantograph model and

z_{cw1} and z_{cw2} the height of the contact point of the first and second contact wire, respectively.

This contact model only takes into account the vertical component of the interaction force. However, in the overlaps there is a longitudinal impact of the contact strip on the overlapping contact wire. According to some preliminary calculations, this impact is expected to be low enough to be neglected, since the contact wire at the impact point is practically horizontal (it is only inclined at an angle of approximately 0.2 °).

To consider contact loss with each contact wire independently, the interaction force with the contact wire i is governed by the following unilateral non-linear behaviour:

$$f_{int}^{ji} = \begin{cases} k_c \left(z_1 - z_{cwi} \right) & \text{if} \quad z_1 > z_{cwi} \\ 0 & \text{if} \quad z_1 \leq z_{cwi} \end{cases} \tag{4}$$

The whole dynamic problem is solved by means of the efficient *offline/online* strategy proposed in [14] with the previous modifications to cope with multiple pantographs interacting with two catenary sections simultaneously. The *offline/online* method is based on the Hilber-Hughes-Taylor (HHT) integration scheme [18] and the non-linearities (dropper slackening and contact losses) are efficiently dealt with by applying an iterative procedure in each time step ($\Delta t = 1$ ms).

The simulation of a single pantograph running at 300 km/h is given as an example of the dynamic results that can be obtained with the extended model with overlap sections. Again, the defining parameters of the overlap section are provided in Table 1. It should be noted the external uplift force f_{ext} applied to each pantograph was appropriately tuned in all the simulations to fulfil the maximum mean interaction force $\bar{f}_{int}$, allowed by the electrotechnical standards [19]:

$$\bar{f}_{int} \leq 70 + 0.00097 v^2 \tag{5}$$

where v is the train's speed expressed in km/h. For a $v = 300$ km/h the mean value of the interaction force should be 157.3 N, which is accomplished by

setting the uplift force $f_{ext} = 166.5$ N for this specific pantograph and catenary models. If any parameters of these models are modified, the uplift force must be recalculated.

The plots in all the examples discussed in this work show the interaction force raw version without any cut-off frequency filter. However, similar conclusions to those presented along this paper are obtained if using a 20 Hz low-pass filtered interaction force as some standards suggest.

In this case, the obtained interaction force is given in the top graph in Figure 5, in which the central and overlap spans can be seen to behave differently. The main feature is the peak force that appears when the pantograph starts to interact with the contact wire in the second catenary section, which reaches 282.8 N. Other differences can be quantified by the interaction force SD obtained for the four central spans $\sigma_c = 26.76$ N, and for the four spans centred on the overlap section $\sigma_o = 28.99$ N, which have a slightly higher fluctuating behaviour. Indeed, the highest value of σ is found in the two spans centred on the overlap section (from 845 m to 975 m), taking a value of 31.10 N. The lower graph in Figure 5 gives the contribution to the interaction force of each contact wire along the overlap section. The pantograph starts interacting with the second contact wire some metres before reaching the crossing point (910 m) and remains in contact with both wires for 13.4 m.

3. Consideration of extra features on the catenary model

Double cantilevers and tensioning efficiency were incorporated in the catenary model to study their contributions to the interaction force and thus, verify if they need to be further considered. As both elements are placed at the ends of a catenary section, any effects on the pantograph-catenary dynamic interaction are expected to occur near the overlap section.

3.1. Simulation of double cantilevers

The three central poles of the overlap section (see Figure 1) are endowed with a double cantilever (see Figure 6) to support the cabling of both catenary

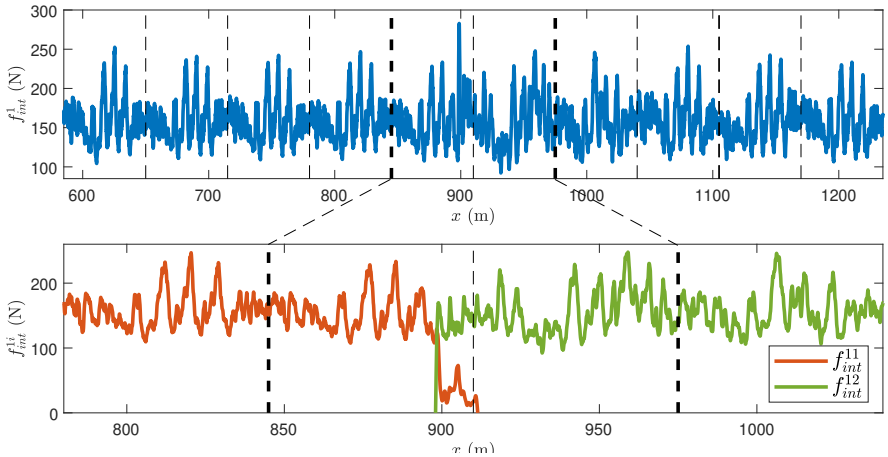

Figure 5: *Total interaction force (top figure) and the contribution of each contact wire (lower figure) in the overlap section.*

sections. One is a fixed bracket without steady arm which constrains the vertical movements of the contact wire.

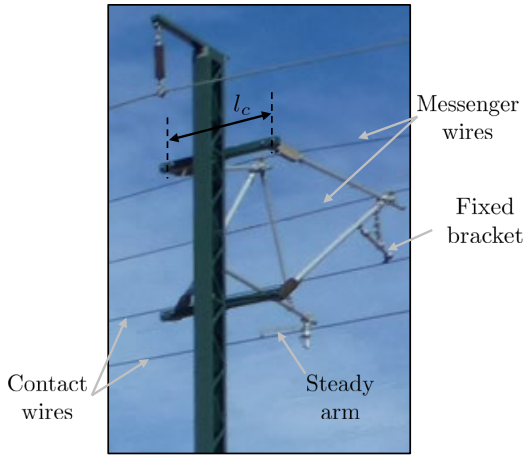

Figure 6: *Photo of a double cantilever on a post in the overlap section.*

Both cantilevers are separated by a distance of l_c, which is usually around 1.5 m. A simulation with two pantographs running at 300 km/h and spaced at 200 m was performed with two different catenary models at values of l_c =

1.5 m and $l_c = 0$ m to evaluate the effect of double cantilevers on the dynamic behaviour of the system. The latter is the usual simplified scenario with the two cantilevers placed at the position of the post. A scheme of the top view of the overlap geometry is provided in Figure 7.

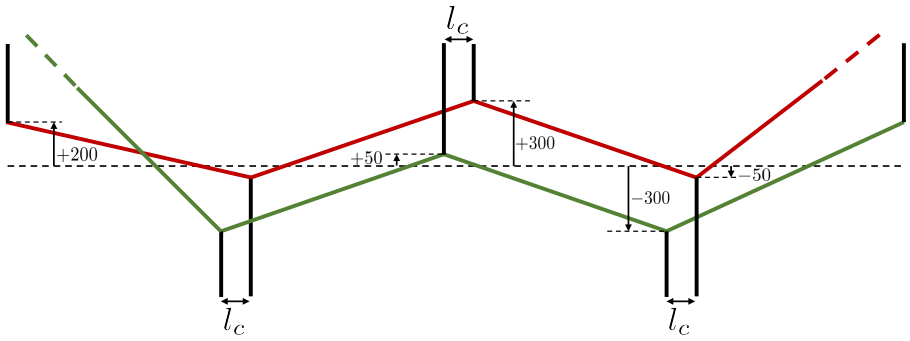

Figure 7: *Schematic top view of the overlap section with double cantilevers separated by a distance of l_c (dimensions in millimetres).*

The interaction force obtained is given in Figure 8 for both front and rear pantographs along the overlap section. Some differences were found between the pantographs, which are more appreciable in the trailing pantograph in the overlap section (from 860 m to 910 m) due to interacting with a catenary previously excited by the leading pantograph. There is also an increase in the peak force when the pantographs start to interact with the second catenary section. Despite these small discrepancies in the interaction force, simulating double cantilevers at the nominal position of the post could remain a valid option, at least when using simple lumped-mass pantograph models with a single contact strip.

3.2. Analysis of tensioning device efficiency

Tensioning devices are installed at the ends of each catenary section to keep the tensile forces constant in the contact line. These systems compensate for variations in the length of the contact and messenger wires due to thermal dilatations. Systems of weights and wheels such as that shown in Figure 9a are

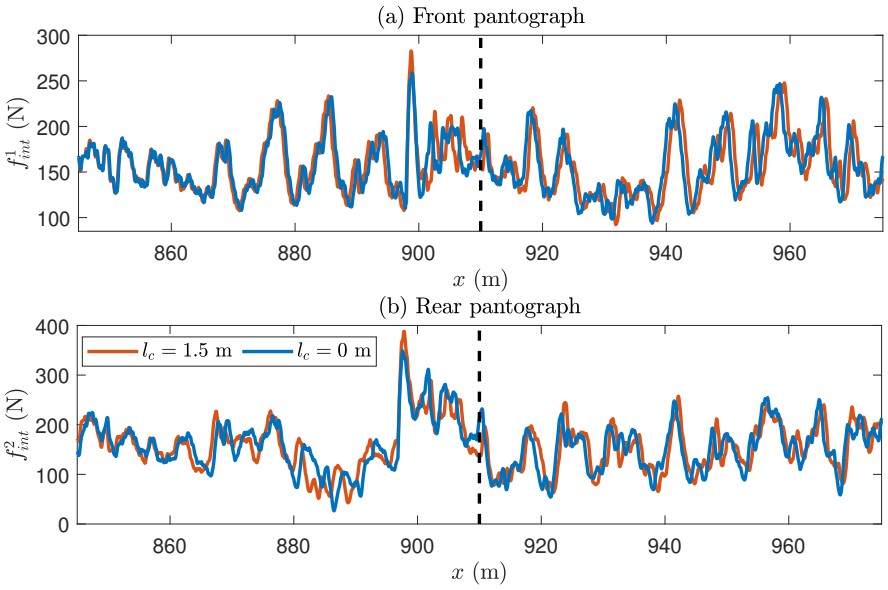

Figure 8: *Interaction force along the overlap section produced by the interaction of the front (a) and rear (b) pantograph with a catenary with double cantilevers spaced at 1.5 m and 0 m.*

widely used for high-speed overhead contact lines.

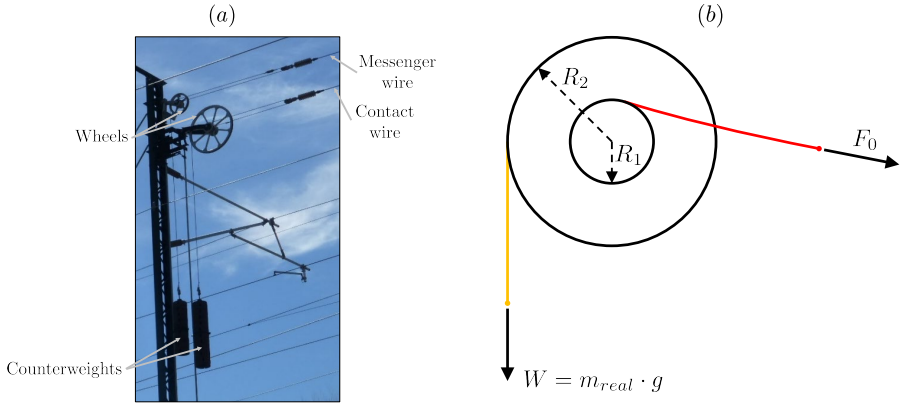

Figure 9: *(a) View of a tensioning device with a system of weights and wheels, and (b) forces acting on wheels and counterweights.*

Considering that the wire holds a nominal tension force F_0, moment equilibrium at wheels' axis (see Figure 9b) leads to:

$$F_0 \cdot R_1 = m_{real}\, g \cdot R_2 + T_f \tag{6}$$

where R_1 and R_2 are the inner and outer wheel radius, m_{real} is the counterweight mass, g the gravity constant and T_f is the torque produced by friction.

The wheel system does not rotate unless the change in F_0 is large enough to overcome the maximum resistive torque, so that for a catenary section i and a certain wire k ($k = \{c, m\}$ for contact and messenger wires respectively) its tensioning device efficiency η_{ki}, is defined as the factor by which the traction force of the wire k, F_{0k}, can be changed without moving the corresponding wheel system, usually within $[0.97 - 1.03]$ according to [1].

Temperature changes can cause sufficient variations in the traction force on the wires to move the tensioning system. However, our simulations revealed that in normal operations the passing of the pantograph only causes minor variations in the wires tension and this is unlikely to move the wheels system. However, even if this movement is allowed for in the model the effect on the dynamic behaviour of the system in minimal.

Regarding the static configuration of the catenary system, the efficiency of the tensioning devices has a major effect, since the actual tension of the wires can be $|\eta - 1|\, F_0$ without being compensated by the movement of the tensioning devices in a catenary section. To simulate this effect, the first step consists of solving the shape-finding problem described in Section 2 with design conditions ($\eta_{ki} = 1$) to obtain the undeformed length of each element of the mesh. The tension force is replaced by $\eta_{ki} F_{0k}$ and a non-linear static equilibrium problem (Eq. (1)) is solved. As a result, the final initial catenary configuration differs from that planned in the design, as depicted in Figure 10 for an extreme scenario in which $\eta_{ki} \in [0.95 - 1.05]$.

An enlarged view of the contact wire reveals that its height varies by at most ± 3 cm at the centre of the span with respect to the nominal height when efficiencies are $\eta_c = \eta_m = 1.05$ and $\eta_c = \eta_m = 0.95$, respectively. If different

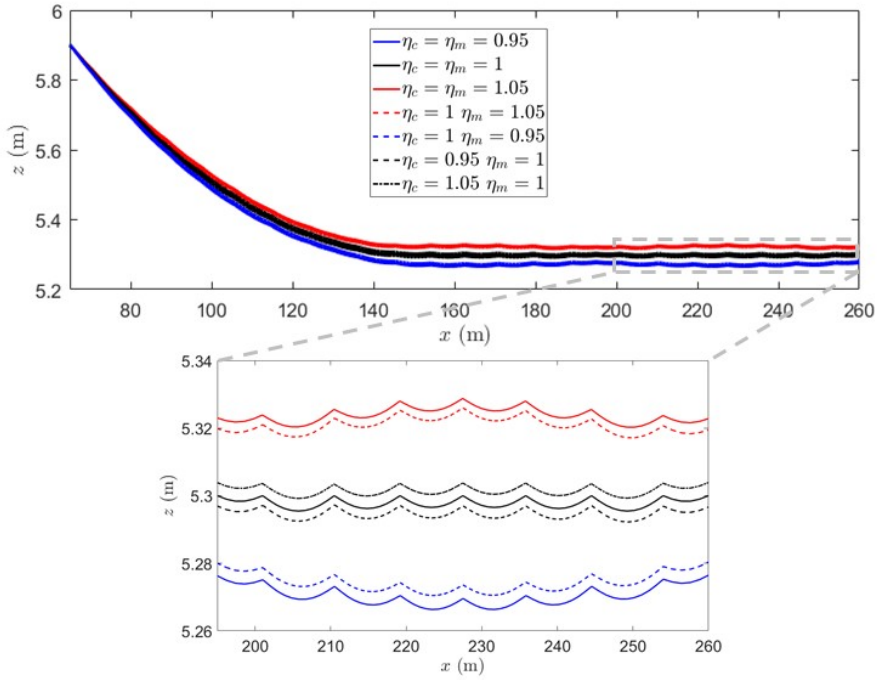

Figure 10: *Contact wire height in catenaries with different tensioning device efficiencies.*

efficiencies are imposed for the contact and messenger wires' tensioning devices ($\eta_c \neq \eta_m$, dashed lines in Figure 10), the variations in contact wire height from the nominal catenary are similar to those with $\eta_c = \eta_m$. These results highlight the fact that contact wire height is more influenced by the efficiency of the messenger wire tensioning devices than by the efficiency of its own tensioning devices.

Regarding the dynamic behaviour of the coupled pantograph-catenary system, it is important to note the effect of changes in the efficiency of the tensioning system on the interaction force. For this, six scenarios were studied from simulations with two overlapped catenary sections whose initial configuration was obtained by considering different tensioning efficiencies. A summary of the results obtained from the different scenarios is given in Table 2, with the SD and maximum value of the interaction force for the front and rear pantographs for

Table 2: *Comparison of the interaction force SD and maximum ($\sigma(f_{int})$, $f_{int,}^{max}$), in a centre and overlap section of the catenary, for the front and rear pantographs in six scenarios combining different tensioning devices efficiencies.*

	Scenario	Nominal	1	2	3	4	5	6
Section 1	CW	1.00	1.05	0.95	0.95	1.05	1.05	0.95
efficiency	MW	1.00	1.05	0.95	1.00	1.00	1.00	1.00
Section 2	CW	1.00	1.00	1.00	0.95	1.05	1.00	1.00
efficiency	MW	1.00	1.00	1.00	1.00	1.00	1.05	0.95
$\sigma_c(f_{int})$	Front	26.76	23.43	27.00	27.83	23.51	23.51	27.83
(N)	Rear	36.50	31.81	45.45	45.47	33.59	33.59	45.47
$\sigma_o(f_{int})$	Front	30.40	30.79	30.80	31.64	29.04	29.47	31.80
(N)	Rear	47.59	51.98	50.64	49.98	45.05	46.32	47.43
$f_{int,c}^{max}$	Front	252.5	235.8	247.5	256.2	229.1	230.2	256.2
(N)	Rear	257.8	243.5	308.8	286.2	229.1	230.2	286.2
$f_{int,o}^{max}$	Front	282.8	302.3	307.5	260.6	285.8	265.9	274.6
(N)	Rear	388.4	491.8	381.2	333.6	401.8	361.7	321.1

the central and overlap spans $\sigma_c(f_{int})$, $f_{int,c}^{max}$ and $\sigma_o(f_{int})$, $f_{int,o}^{max}$, respectively.

The main conclusion drawn from these results is the remarkable influence of tensioning devices efficiency on the dynamic behaviour of the coupled pantograph-catenary system, not only on the overlap spans ($x \in [845, 975]$ m) but also in the central spans due to the change in the initial configuration. The results also reflect the great complexity of the pantograph-catenary dynamic interaction, especially in the overlap section (see Figure 11), since none of the six scenarios simulated produced either an overall benefit or disadvantage.

4. Effect of train speed on the overlap sections

Higher train speeds are known to reduce current collection quality. This phenomenon has been widely studied in the literature (see for example [20, 21])

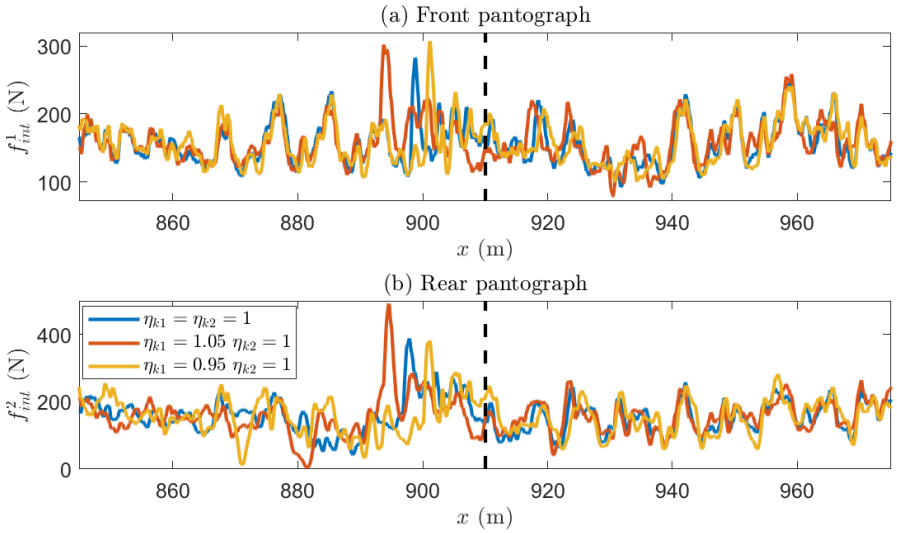

Figure 11: *Force produced by the interaction of the front (a) and rear (b) pantographs in two catenary sections with different efficiencies.*

for the central spans of a catenary section. However to the best of our knowledge no work has been done on transitions between two catenary sections.

A number of simulations were performed with the nominal catenary and a pantograph running at speeds between 200 km/h to 340 km/h. The interaction force SD for each speed is shown in Figure 12, in which the dashed lines refer to central spans while the solid lines represent overlap spans. This analysis also considered both front (circle markers) and rear (cross markers) pantographs.

Figure 12 shows the increase of $\sigma(f_{int})$ when the train speed rises. A greater $\sigma(f_{int})$ is obtained in the overlap section than in the central spans not only for the nominal speed, as concluded in Section 2, but also for the entire speed range. The slight difference in the front pantograph between $\sigma(f_{int})$ in the overlap and central spans remains almost constant with speed, showing that the slightly negative effect on current collection quality in the overlap sections at higher $\sigma(f_{int})$ is the same at 200 km/h as at 340 km/h. In the rear pantograph, a higher increment is observed which varies with speed.

Another important aspect to consider is the statistical minimum value of

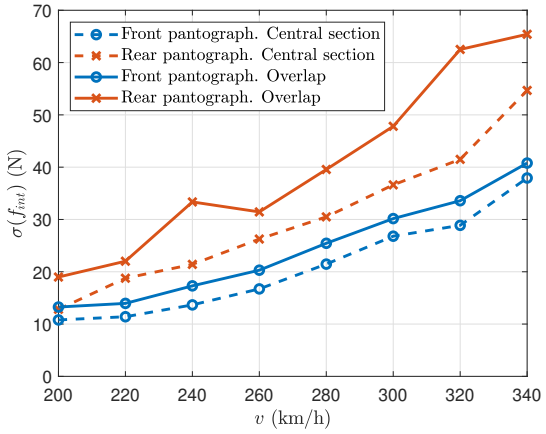

Figure 12: *Evolution of interaction force SD with train speed in central and overlap sections for both front and rear pantographs.*

the interaction force in the overlap section, since it increases the probability of contact losses and arcing. Figure 13a shows magnitude (solid line) versus train speed. Although a small increase in minimum interaction force is apparent at high speeds in the front pantograph, which could be viewed as a positive trend, in fact the statistical minimum computed as $(\bar{f}_{int} - 3\sigma(f_{int}))$ remains almost constant (dashed lines in Figure 13a). On the other hand, in the rear pantograph both real and statistical minima fall below zero, which reveals the higher chance of contact losses at high speeds in the overlap section, especially for $v > 300$ km/h.

In Figure 13b variations of the maximum interaction force $\max(f_{int}^{ji})$ in the overlap section of pantograph j and contact wire i are given in relation to speed. The general trend indicates increasing values as speed rises. It should be noted that the maximum contact force between the front pantograph and the second contact wire $\max(f_{int}^{12})$ is higher than that with the first contact wire $\max(f_{int}^{11})$ for the entire speed range. These results indicate that higher wear rates can be expected in the first spans of a catenary section.

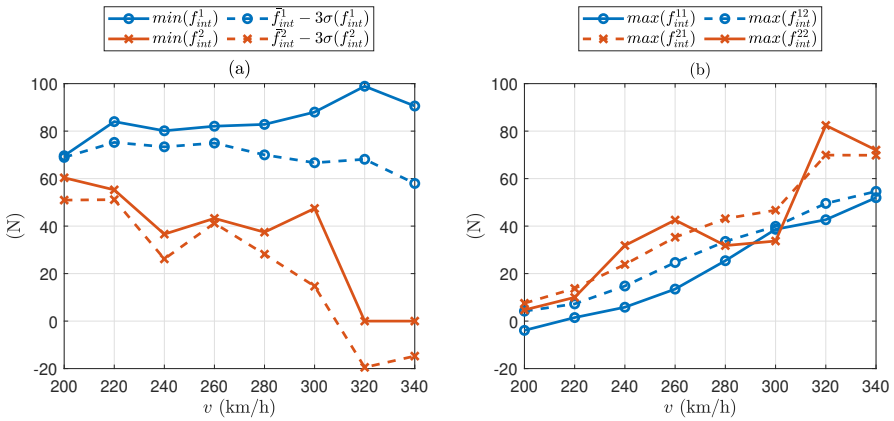

Figure 13: *(a) Real and statistical minimum interaction force of both pantographs and (b) maximum interaction force $max(f_{int}^{ji})$, between pantograph j with contact wire i in the overlap section.*

5. Parametric analysis of the overlap contact wire height

A parametric analysis was performed with $h_1 \in [0.1, 0.7]$ m and $h_2 \in [0, 0.06]$ m to study the influence of the contact wire height profile in the overlap section on the pantograph-catenary coupled dynamics. As defined in Figure 2, h_1 and h_2 are the contact wire heights at the supports on the overlap section. According to [19], there must be a clearance of $2S_0$ between the moving steady arm and the cantilever structure, where S_0 is a value defined by the infrastructure provider (12 cm in Spanish high-speed lines) which corresponds to the maximum steady arm uplift when the pantograph passes. This clearance can be reduced to $1.5S_0$ if the steady arms are equipped with an uplift stop. The actual maximum value of the lower limit of h_1 in high-speed catenaries is then obtained by the addition of the pantograph gauge with the necessary space to arrange the rods of the double cantilever. As can be seen in Figure 14, all these premises lead to $h_1 > 0.45$ m as the maximum lower limit of h_1. However, in this analysis the lower limit in h_1 was reduced to $h_1 > 0.1$ m to study the dynamic behaviour of the system in a wider scenario.

As in the previous examples, the simulations were performed with two pan-

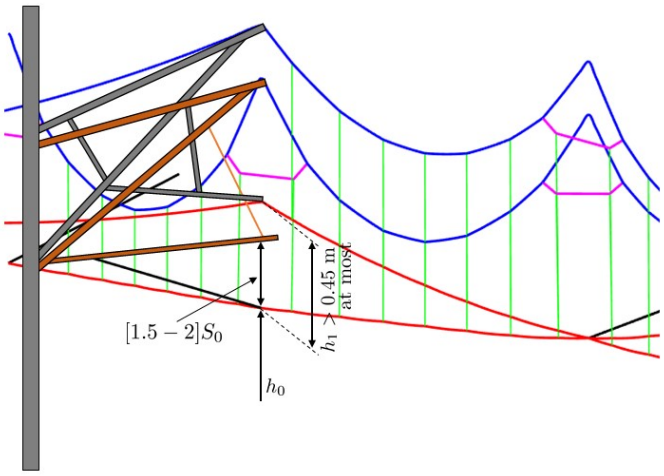

Figure 14: *Schematic view of a double cantilever in the overlap section. Pantograph gauge and spatial limitation of the height of the fixed point* h_1.

tographs separated by 200 m running at 300 km/h. Figure 15 shows the interaction force SD, $\sigma(f_{int})$, as a function of h_1 and h_2, as in Figure 16 for the maximum interaction force and Figure 17 for its statistical minima. These magnitudes were measured in the three spans containing the crossing point of the contact wires of two sections for both front and rear pantographs. It is important to note that some points were removed (those with minimum h_1 and high h_2) due to interaction with the anchoring spans.

As a general observation, the height of the fixed bracket, h_1, is the most influential of the two parameters studied, while the crossing point height h_2 has little influence, especially for low h_1 values beyond the limit of 0.45 m (highlighted by a red line).

In view of the results obtained, the optimal geometry of the overlap spans is that in which $h_1 = 0.1$ m and $h_2 \in [0,\ 0.035]$ m, not only for the front pantograph but also for the rear, because the interaction force shows the lowest SD values and maximum and the highest statistical minimum value. As pointed out above, there is a technical limit in h_1 which is shown as a red line in Figure 15. Its nominal value is $h_1 = 0.6$ m (marked with a red point in Figure 15), and there is

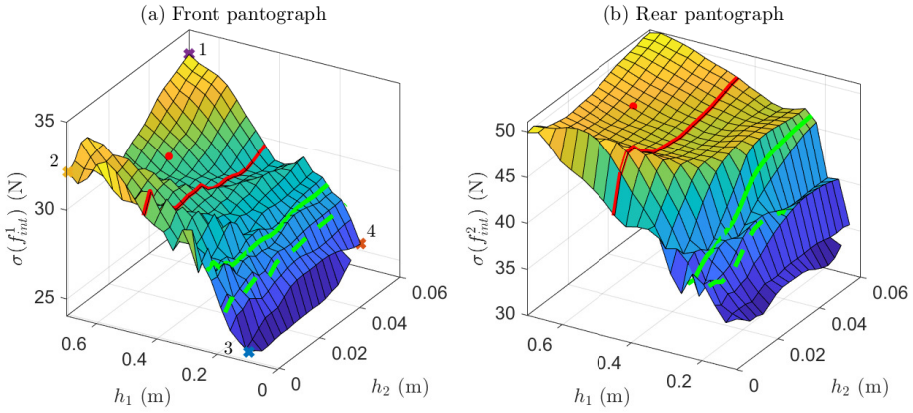

Figure 15: *SD of the interaction force measured in the three spans centred on the crossing point. (a) Front and (b) rear pantograph.*

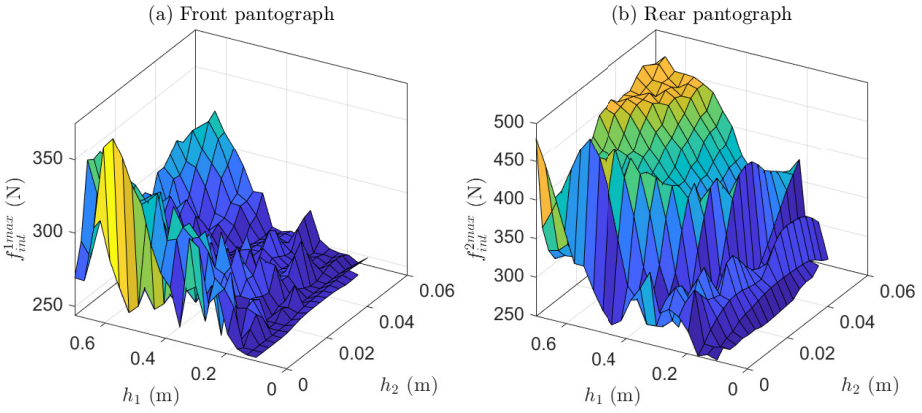

Figure 16: *Maximum interaction force measured in the three spans centred on the crossing point. (a) Front and (b) rear pantograph*

.

therefore great room for improvement by installing new bracket configurations to reduce h_1 closer to the pantograph gauge limits (green solid and dashed lines in Figure 15), as long as it is an electrically connected overlap. Nonetheless, in the case of insulating overlaps, an air-gap distance (0.3-0.45 m) must always be kept between the two contact wires.

For a deeper analysis of the results, the focus was put on four different

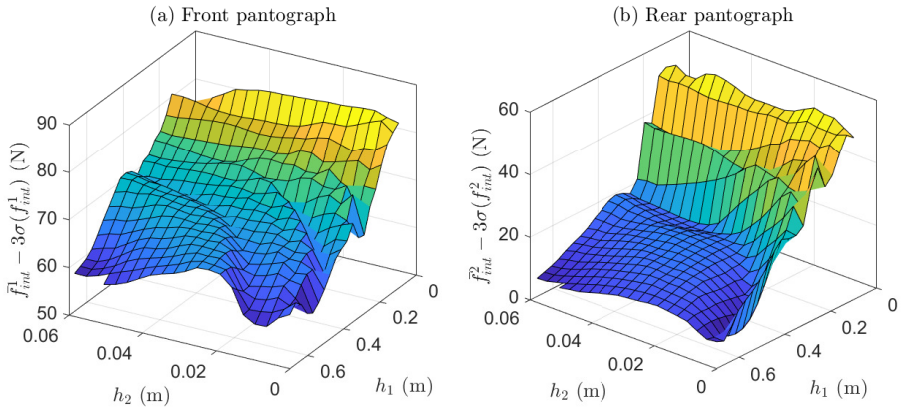

Figure 17: *Statistical minimum interaction force measured in the three spans centred on the crossing point. (a) Front and (b) rear pantograph*

.

contact wire profiles selected from the parametric space, matching its four limits (numbered points marked with crosses in Figure 15a). The contact wire height on the two central overlap spans for these four points of the parametric space is plotted in Figure 18.

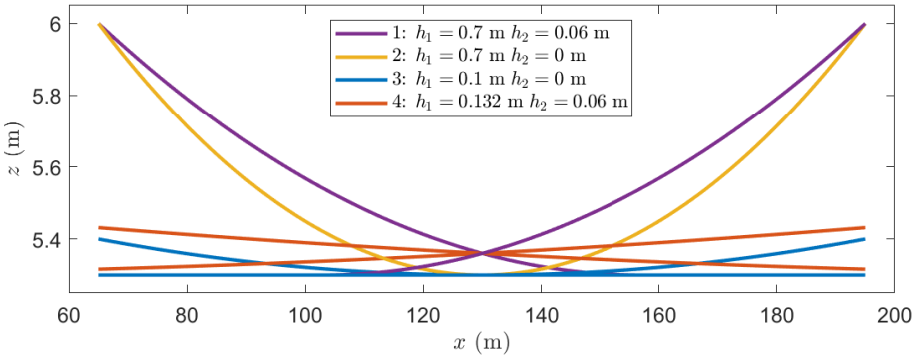

Figure 18: *Contact wire height in the overlap section for the four parametric space limits* (h_1, h_2).

Figure 19 gives the interaction force between the front pantograph and both contact wires in the overlap section. The points at which the pantograph starts

interacting with the second wire (top graph) and stops interacting with the first wire (bottom graph) are highlighted with vertical dashed lines. The interval between these two lines is the distance in which the pantograph is in contact with both wires. Note that this interval must be within the limits [845, 975] m of the fixed bracket positions since the pantograph cannot interact with the anchoring spans.

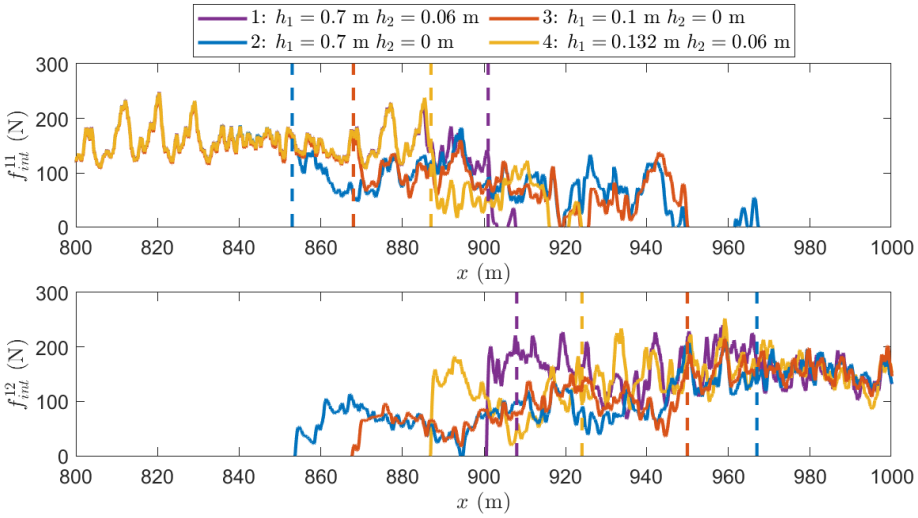

Figure 19: *Interaction force between front pantograph and contact wire of the ending catenary section (top) and the starting catenary section (bottom) in the overlap section.*

There is a direct relationship between this distance and the dynamic performance of the system, since the longer the pantograph is in contact with both wires, the lower the interaction force SD, the lower its maximum value and the higher its statistical minimum. These reduced fluctuations in the interaction force at low h_1 values could be associated with the fact that the interaction with both contact wires begins and ends more gradually because the slope of the wires is smaller, although this also causes some contact losses, especially with the first contact wire.

The previous parametric analysis of the overlap contact wire height was performed on catenary sections whose tensioning devices compensated for nominal

wire tension, even though, as mentioned in Section 3.2, this is not common in a realistic set-up and may have a significant impact on the current collection quality. To clarify the relationship between contact wire height in the overlap section and the efficiency of the tensioning devices, the different values within the parameter (see Figure 15) are repeated here for two overlapped catenary sections with $\eta_{c1} = \eta_{m2} = 0.95$ and $\eta_{c2} = \eta_{m1} = 1$ (one of the worst cases in Table 2 for the front pantograph in the overlap section) and compared in Figure 20.

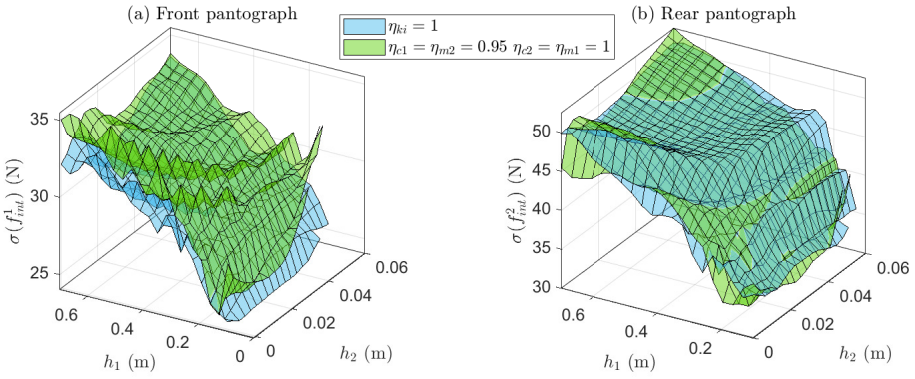

Figure 20: *Standard deviation of the interaction force measured on three spans centred on the overlap region for the nominal catenary and a catenary with different tensioning device efficiencies. (a) Front pantograph and (b) rear pantograph.*

In view of the results obtained, the front pantograph's $\sigma(f_{int}^1)$ is greater than that obtained for the nominal catenary at all the studied values of parameters h_1 and h_2. For the rear pantograph, the lowest $\sigma(f_{int}^2)$ is obtained for one or other catenary according to the values of h_1 and h_2. However, both pantographs show a similar tendency to the reference case for changes in parameters h_1 and h_2, so that reducing h_1 to the minimum is also applicable to actual catenaries with non-unitary efficiency of the tensioning devices.

6. Three, four and five-span overlap sections

The case of four-span overlap sections (common to many existing catenaries) was thoroughly analysed in this study. However, some catenaries have three or five-span overlap sections, which guarantee pantograph contact with both contact wires at the centre region of the span instead of at the supports (see Figure 21).

On purely economic grounds, three-span overlaps are the cheapest solution for obvious reasons, although they cannot be installed in high-speed catenaries with high contact wire mechanical tension and the usual span lengths, because it is not possible to raise the contact wire sufficiently at the supports while keeping it at an appropriate height at the crossing point.

This is why four-span overlaps are the common solution in high-speed catenaries. However, if the length of the span at which the contact wire rises is too short (usually $L_s < [50 - 55]$ m) it is difficult to achieve the desired height (h_1) at the supports. In this case, the usual solution is to adopt five-span overlaps.

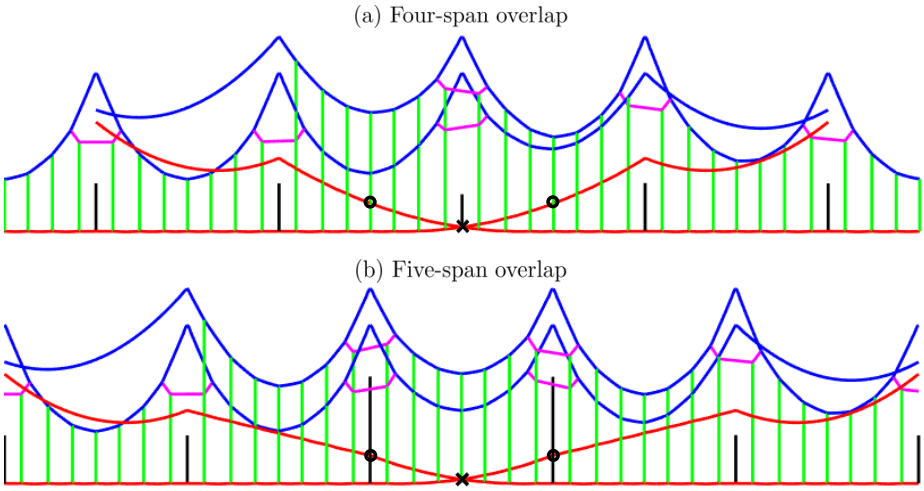

Figure 21: *(a) Four and (b) five-span overlap sections with identical contact wire height in a span length centred at the crossing point.*

The focus was on comparing the dynamic behaviour of four and five-span

overlaps. In order to make the two models as comparable as possible, the nominal four-span overlap catenary was selected and for the five-span overlap catenary the crossing point was set at 0.035 m above the nominal height (shown as crosses in Figure 21), while the contact wire points at a half-span from the crossing point are held at 0.231 m above the nominal height (depicted as circles in Figure 21). The contact wire height profile in the region of a span length (65 m) centred at the crossing point was therefore the same for both models.

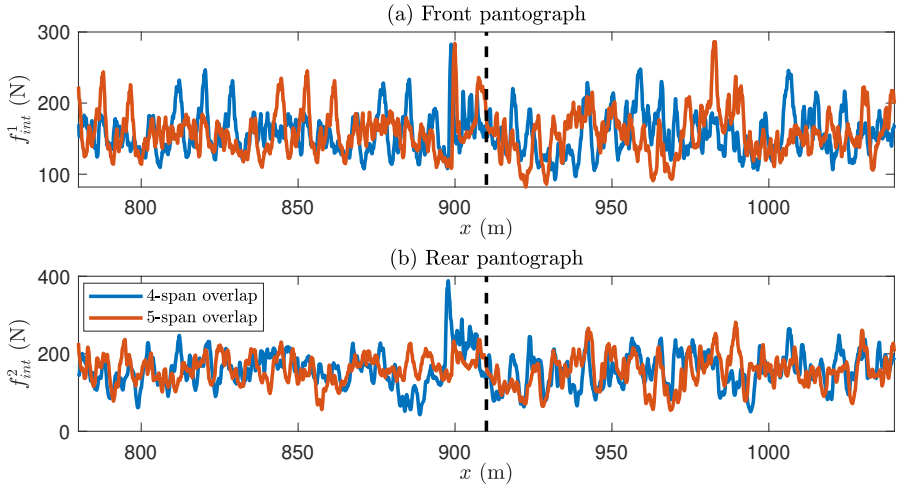

Figure 22: *Interaction force between front (a) and rear (b) pantographs and catenaries with 4 and 5-span overlap sections.*

The pantograph-catenary dynamic interaction was simulated with the same settings as in the previous examples to obtain the interaction force (see Figure 22). The contact force of the five-span overlap model was offset so that the x coordinate of the crossing point (vertical dashed line) matched in both cases.

The fluctuations of the interaction force measured in the three spans centred at the crossing point lead to $\sigma(f^1_{int_{4s}}) = 30.40$ N for the front pantograph in the nominal catenary and $\sigma(f^1_{int_{5s}}) = 32.06$ N in the five-span overlap catenary model. This greater $\sigma(f_{int})$ can be seen in Figure 22a, as well as the lower minima and higher peak force in the first spans of the second catenary section. The rear pantograph behaved rather better in the five-span overlap

section, as revealed by the lower $\sigma(f^2_{int_{5s}}) = 40.65$ N and $f^{2max}_{int_{5s}} = 279.2$ N if compared to the nominal values $\sigma(f^2_{int_{4s}}) = 47.59$ N and $f^{2max}_{int_{4s}} = 388.4$ N (see Figure 22b). There was thus a slight deterioration of the leading pantograph's current collection quality and a notable improvement of this magnitude in the trailing pantograph in five-span overlaps. Along with other factors, such as geometric design constraints or economic costs, these results could be used to tip the balance in favour of either solution.

7. Optimisation of a catenary section geometry

According to the literature, contact wire height and dropper spacing are the two geometrical factors which greatly influence the dynamic performance of the catenary system. Although previous studies [15] proposed optimal values of these parameters to obtain the most uniform interaction force by minimising their SD, these optimisations only focused on the central spans and were solved by means of a Genetic Algorithm (GA) considering a maximum of five optimisation variables.

In the present work, the optimisation of an entire catenary section, including the transition spans, was carried out by means of a Bayesian Optimisation (BO) technique [22]. The main advantage of BO algorithms in this problem is that fewer evaluations of the objective function (OF) are required than with GA (around 20 times fewer [23]), which means more optimisation variables can be included at a reasonable computational cost.

On the premise that all spans have seven droppers and must be equal and symmetric, the set of nine variables to be optimised includes the distance between droppers x_1, x_2 and x_3 (see Figure 2), the contact wire height at dropper connection points h^1_d, h^2_d, h^3_d and h^4_d, and the supports' heights h_1 and h_2 from which a parabolic profile is defined for the contact wire in the overlap section. They can be grouped as:

$$\mathbf{p} = [x_1 \ x_2 \ x_3 \ h^1_d \ h^2_d \ h^3_d \ h^4_d \ h_1 \ h_2] \tag{7}$$

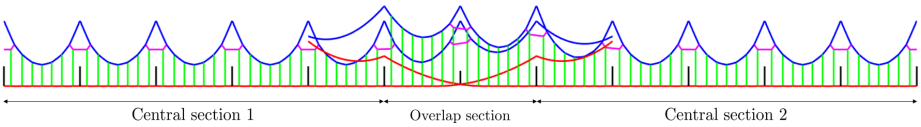

Figure 23: *Entire catenary section, including a transition, used for the optimisation problem.*

The entire catenary section to be optimised is shown in Figure 23. It contains 12 spans; five central spans in Section 1, a further five are central spans in Section 2 and the last two belonging to the overlap section. The optimisation problem therefore reads:

$$\begin{aligned} &\min_{\mathbf{p}} \quad OF(\mathbf{p}) = \sigma_c\left(f_{int}\right) + 5\sigma_o\left(f_{int}\right) \\ &\text{s. t.} \\ &p_i^{min} \leq p_i \leq p_i^{max} \quad i = 1, ..., 9 \end{aligned} \tag{8}$$

where σ_c is the SD of the interaction force in the central Sections 1 and 2, σ_o is the SD of the interaction force in the overlap section and each of the optimisation parameters (7) are discretised and bounded. Note that σ_o was weighted by a factor of five to compensate for being measured in only two spans, unlike σ_c, which was obtained in 10 spans. To solve the optimisation problem (8), additional constraints were considered by penalising the OF when they are active. These constraints were:

- $\mathbf{p}^{min} = [0.1\ \ 9.1\ \ 20.5\ \ -0.01\ \ -0.015\ \ -0.02\ \ -0.02\ \ 0.1\ \ 0]$
- $\mathbf{p}^{max} = [9\ \ 20.4\ \ 32.4\ \ 0.01\ \ 0.015\ \ 0.02\ \ 0.02\ \ 0.7\ \ 0.06]$
- Slackened droppers are not allowed in the initial configuration.
- The pantograph cannot interact with the second catenary section before the overlap section nor with the first catenary section after the overlap section.
- Contact losses are not accepted.

With this setup the MATLAB® built-in BO algorithm with default options was run, reaching 1000 evaluations of the OF. Figure 24 shows that the optimum

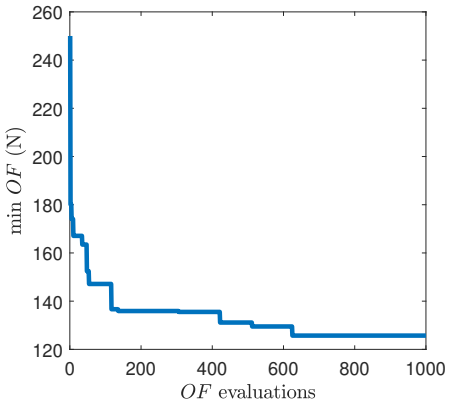

Figure 24: *Minimum objective trace at each evaluation of the OF.*

was found after 620 evaluations and this value was not further updated in the remaining evaluations, confirming the ideal performance of BO algorithms for this problem.

The best geometry was found to be the catenary initial configuration shown in Figure 25, which also gives the optimal dropper distribution and contact wire height in the span. The optimal parameter values $\mathbf{p}$ are compared with those of the nominal catenary in Table 3.

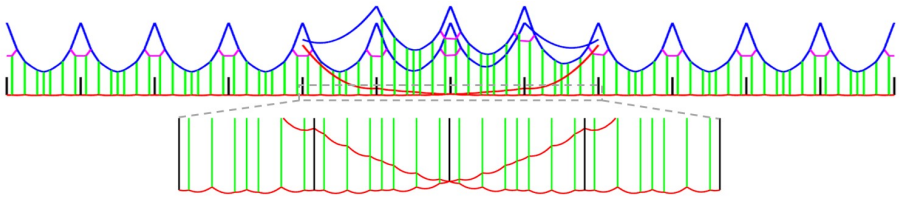

Figure 25: *Optimised catenary initial configuration with zoom view of contact wire height.*

Table 3 also shows the dynamic response of the system quantified by interaction force statistical parameters for the central, overlap and the entire catenary sections. The results show a significant reduction of the interaction force SD, not

Table 3: *Comparison between the nominal and the optimised catenaries.*

	Nominal catenary	Optimised catenary	Inprovement (%)
x_i	6.00 9.48 8.70	4.72 11.13 10.97	-
h_d^i	0 0 0 0	0 0.006 -0.004 0.001	-
h_i	0.6 0.035	0.12 0.017	-
$\sigma_c(f_{int})$ (N)	26.76	16.60	37.97
$\sigma_o(f_{int})$ (N)	30.40	23.29	23.39
$\sigma_{tot}(f_{int})$ (N)	27.45	18.54	32.46
f_{int}^{max} (N)	282.83	246.9	12.7
$\bar{f}_{int} - 3\sigma_{tot}(f_{int})$ (N)	74.95	101.68	35.66
Δz_{ra}^{max} (cm)	10.54	9.11	13.57

only in the central spans ($\sigma_c(f_{int})$) but also in the overlap section ($\sigma_o(f_{int})$), reaching more than 32% of decrease in the whole section ($\sigma_{tot}(f_{int})$), which would allow the uplift force to be reduced in the optimised catenaries without increasing the risk of contact losses. The maximum value of the interaction force f_{int}^{max} is almost 13% lower in the optimised catenary, its statistical minimum $\bar{f}_{int} - 3\sigma_{tot}(f_{int})$ is 35% higher and the maximum uplift of any registration arm Δz_{ra}^{max} is 13.5% lower. These results indicate that the optimised catenary section performs much better than the nominal catenary.

Figure 26 gives a comparison of the interaction force obtained with the nominal and optimised catenaries. The overlap section bounds are marked with dashed lines. In this case, the most striking feature is the significant reduction of the peaks in the optimised catenary. However, despite the intrinsic complexity of the pantograph-catenary dynamic interaction, benefits in the optimised catenary response are found at other train speeds and in other catenaries such as those without stitched wires.

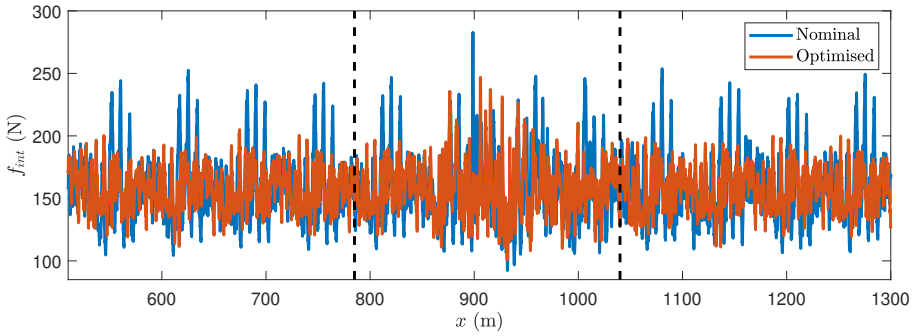

Figure 26: *Comparison of interaction force obtained with nominal and optimised catenaries.*

8. Conclusions

This paper describes a detailed analysis of the pantograph-catenary dynamic interaction in the overlap sections in two-pantograph operations. Although the results were obtained from a model based on the EAC-350 catenary, the proposed methodology is valid for any other type.

The transitions between two tensioning sections are revealed as the most critical in terms of current collection quality as measured by the interaction force SD. This behaviour was found in a wide range of train speeds in which the interaction force peak values increase with speed while the minimum force values tend to stay constant or even decrease with speed.

The effect of incorporating double cantilevers was checked to give the models more realistic features. According to the results obtained, these elements do not appear to be significant with barely any differences in the interaction force of both front and rear pantographs.

However, if tensioning devices are included in the models as non-ideal components with mechanical losses, important effects are found in the initial configuration of the catenary and consequently in its dynamic behaviour. The efficiency of the messenger wire tensioning devices has a remarkable influence on contact wire height, which is lower than its nominal value for efficiencies below one and vice versa.

With respect to the contact wire height profile on the overlap spans, the parametric analysis revealed that the height of the contact wire anchoring point on the end support should be as low as possible to reduce interaction force fluctuations in both pantographs, also when deviations from the nominal efficiency of the tensioning devices are considered.

The possibility of installing four or five-span catenary overlaps was also studied and their dynamic behaviour compared by numerical simulations. Considering only mechanical factors, five-span overlaps are slightly detrimental to current collection in the leading pantograph but markedly beneficial in the trailing collector.

The Bayesian Optimization technique proposed in this paper is more efficient than other optimization methods such as the Genetic Algorithms [15] since it needs fewer objective function evaluations. The optimal contact wire height for the central and overlapping spans and dropper spacing were found, leading to a catenary that provides an interaction force with a more than 32% lower SD. The optimised catenary section enables a lower maximum and higher minimum interaction force, while the maximum steady arms uplift is reduced by 13.5% compared to the values obtained with the nominal catenary.

These results and conclusions are strictly only applicable for the examples used in the simulations performed in this work and experimental validation is still required to corroborate them. However, they do contribute information, guidelines and trends which can be used in a more general sense by catenary designers and infrastructure managers.

Acknowledgements

The authors would like to acknowledge the financial support received from the Regional Government of Valencia (PROMETEO/2016/007) and the Spanish Ministry of Economy, Industry and Competitiveness (TRA2017-84736-R). The funds received jointly from the Regional Government of Valencia and the European Social Fund under Grant APOSTD/2019/205 are also acknowledged.

The authors wish to express their gratitude for the comments and useful information provided by José Antonio Martínez López and the 'Sociedad Española de Montajes Industriales' (SEMI Group).

References

[1] F. Kiessling, R. Puschmann, A. Schmieder, E. Schneider, Contact lines for electrical railways: Planning, Design, Implementation, Maintenance, 3rd Edition, Publicis Publishing, Erlangen, Germany, 2018.

[2] S. Bruni, J. Ambrósio, A. Carnicero, Y. H. Cho, L. Finner, M. Ikeda, S. Y. Kwon, J. P. Massat, S. Stichel, M. Tur, The results of the pantograph-catenary interaction benchmark, Vehicle System Dynamics 53 (3) (2015) 412–435.

[3] Z. Liu, Y. Song, Y. Han, H. Wang, J. Zhang, Z. Han, Advances of research on high-speed railway catenary, Journal of Modern Transportation (2016) 1–23.

[4] S. Bruni, G. Bucca, M. Carnevale, A. Collina, A. Facchinetti, Pantograph–catenary interaction: recent achievements and future research challenges, International Journal of Rail Transportation (2017) 1–26.

[5] P. Antunes, J. Ambrósio, J. Pombo, A. Facchinetti, A new methodology to study the pantograph–catenary dynamics in curved railway tracks, Vehicle System Dynamics (2019) 1–28.

[6] M. Shimizu, Y. Fujii, Improvement of structure of contact wire on overlap sections of Shinkansen, Quarterly Report of RTRI 41 (4) (2000) 159–162.

[7] P. Harell, L. Drugge, M. Reijm, Multiple pantograph operation-effects of section overlaps, in: The dynamics of vehicles on roads and on tracks. Proceedings of the 18^{th} IAVSD symposium held in Kanagawa, Japan, 2004.

[8] P. Harell, L. Drugge, M. Reijm, Study of critical sections in catenary systems during multiple pantograph operation, Proceedings of the Institution of Mechanical Engineers, Part F: Journal of Rail and Rapid Transit 219 (4) (2005) 203–211.

[9] J. Massat, J. Laine, A. Bobillot, Pantograph–catenary dynamics simulation, Vehicle System Dynamics 44 (sup1) (2006) 551–559.

[10] G. Mei, W. Zhang, H. Zhao, L. Zhang, A hybrid method to simulate the interaction of pantograph and catenary on overlap span, Vehicle System Dynamics 44 (sup1) (2006) 571–580.

[11] J. Benet, A. Alberto, E. Arias, T. Rojo, A mathematical model of the pantograph-catenary dynamic interaction with several contact wires., International Journal of Applied Mathematics 37 (2) (2007).

[12] P. Antunes, J. Ambrósio, J. Pombo, M. Pereira, Dynamic analysis of the pantograph-cantenary, interaction on overlap sections for high-speed railway operations, in: The Second International Conference on Railway Technology: Research, Development and Maintenance, Civil-Comp Press, 2014, p. 142.

[13] M. Tur, E. García, L. Baeza, F. Fuenmayor, A 3D absolute nodal coordinate finite element model to compute the initial configuration of a railway catenary, Engineering Structures 71 (2014) 234–243.

[14] S. Gregori, M. Tur, E. Nadal, J. Aguado, F. Fuenmayor, F. Chinesta, Fast simulation of the pantograph-catenary dynamic interaction, Finite Elements in Analysis and Design 129 (2017) 1–13.

[15] S. Gregori, M. Tur, E. Nadal, F. J. Fuenmayor, An approach to geometric optimisation of railway catenaries, Vehicle System Dynamics 56 (8) (2018) 1162–1186.

[16] Y. Song, Z. Liu, H. Wang, X. Lu, J. Zhang, Nonlinear modelling of high-speed catenary based on analytical expressions of cable and truss elements, Vehicle System Dynamics 53 (10) (2015) 1455–1479.

[17] EN 50318, Railway applications. Current collection systems. Validation of simulation of the dynamic interaction between pantograph and overhead contact line, European Union Agency for Railways (2003).

[18] H. M. Hilber, T. J. R. Hughes, R. L. Taylor, Improved numerical dissipation for time integration algorithms in structural dynamics, Earthquake Engineering & Structural Dynamics 5 (3) (1977) 283–292.

[19] EN 50367, Railway applications. Current collection systems. Technical criteria for the interaction between pantograph and overhead line, European Committee for Electrotechnical Standardization (2012).

[20] A. Collina, S. Bruni, Numerical simulation of pantograph-overhead equipment interaction, Vehicle System Dynamics 38 (4) (2002) 261–291.

[21] Y. H. Cho, K. Lee, Y. Park, B. Kang, K. N. Kim, Influence of contact wire pre-sag on the dynamics of pantograph–railway catenary, International Journal of Mechanical Sciences 52 (11) (2010) 1471–1490.

[22] J. Mockus, Bayesian approach to global optimization: theory and applications, Vol. 37, Springer Science & Business Media, 2012.

[23] S. Gregori, M. Tur, A. Pedrosa, F. Fuenmayor, The use of Bayesian Optimisation techniques for the pantograph-catenary dynamic interaction stochastic problem, in: International Conference on Engineering Optimization, Springer, 2018, pp. 997–1008.